

Bulging and bending of Kelvin-Helmholtz billows controlled by symmetry and phase of initial perturbation

E Kit, D Gerstenfeld, A Y Gelfgat,

School of Mechanical Engineering, Faculty of Engineering, Tel-Aviv University,
69978 Tel-Aviv, Israel

N V Nikitin

Institute of Mechanics, Moscow State University, 119899 Moscow, Russia

E-mail: gelfgat@eng.tau.ac.il, kit@eng.tau.ac.il

Abstract

A computational study of two possible modes of instability of developed Kelvin-Helmholtz (KH) billows is carried out. It is shown that depending on one of three factors, (i) symmetry of initial perturbation in the cross-flow direction, (ii) phase shift of initial perturbation in the streamwise direction, or (iii) excitation of either spanwise or oblique initial wave, the resulting instability can set in as a spanwise bending or bulging of a two-dimensional KH roller. To ensure that the observed secondary bifurcations result from the linear instability the study is carried out considering a two-dimensional flow combined of a distorted mean flow and developed “frozen” KH billow in under and/or over-saturated state as a base flow subject to three-dimensional instabilities.

1. Introduction

The present paper is devoted to study of secondary three-dimensional instabilities of Kelvin-Helmholtz (KH) billows that take place qualitatively similar to instabilities of Stuart vortices studied by Pierrehumbert and Widnall [1] and later by Schoppa et al. [2]. Pierrehumbert and Widnall [1] found three different modes of the Stuart vortex instability. The first one corresponds to subharmonic instabilities caused by mutual rollup and pairing of two-dimensional KH billows while “pairing” was attributed to development of two-dimensional billows at subharmonic frequency and “helical pairing” mode corresponds to the three-dimensional billows at subharmonic frequency too. The second, three-dimensional mode, called “translative”, corresponds to a bending of primary two-dimensional billows at fundamental frequency. Later it was studied by Rogers & Moser [3] who called it “bending mode”. The third mode, also three-dimensional and occurring at fundamental frequency, had a smaller growth rate and was not studied in detail in [1]. Later, Schoppa et al. [2,4] showed that this mode can be triggered by a certain initial disturbance and called it “core dynamics instability”. They showed that time evolution of this mode causes bulging of initially two-dimensional spanwise vorticity surfaces, so that in the following text we call it “bulging mode”.

The spanwise undulations of KH rollers, possibly corresponding to the bending instability, were observed in many experiments, e.g., [5-12]. In several three-dimensional numerical studies, e.g., [14-16], initially two-dimensional KH billows arrived to a wavy spanwise pattern, also indicating that the bending instability is probably the fastest growing 3D mode.

Rogers & Moser [3] concluded that secondary three-dimensional instabilities of KH billows develop either after oversaturation of two-dimensional rollers, or after their pairing. They stated in the summary: “Long-term growth of three-dimensionality requires long-term presence of spanwise vorticity in the braid region. In a developing layer, this occurs only at late time, after oversaturation of the two-dimensional rollers. The translative instability is thus an instability of the late-time oversaturated flow. Oversaturation can be prevented when the mixing layer is pairing”. Schoppa et al. [4] observed that initial growth of the bulging mode, called also core dynamic instability (CDI), is interrupted by pairing after which the bulging mode is stabilized. Then growth of this mode was observed again after the pairing. Schoppa et al. [4] concluded that “... for linear 3D perturbation evolution in the presence of pairing, excitation of CDI by subharmonic oblique modes generates three-dimensionality which is comparable to that of nearly the most unstable translative mode”. Seemingly, these conclusions were never questioned. In their detailed study of bulging, or CDI, instabilities Schoppa et al. [2] considered the 2D mixing layer flow during or after KH billows pairing. At the same time in the above cited studies the bending and bulging instabilities were addressed to similar instabilities of Stuart vortex [1,2]. Our recent experiments [12] and computations, which we describe below, show a clear evidence of both bending and bulging instabilities (see Fig. 1) that develop well before pairing. This motivates our revisiting of this problem. In the following we show that by a controlled initial perturbation it is possible to trigger either bending or bulging mode. Selection of either a bulging or bending mode depends on a combination of three following factors: perturbation symmetry in the cross-flow direction, location of a maximum of the perturbation amplitude inside the roller or inside the braid, i.e., on the streamwise phase, and on excitation of either a spanwise or an oblique wave. An alteration of one of these three factors leads to a replacement of bending by bulging or vice versa.

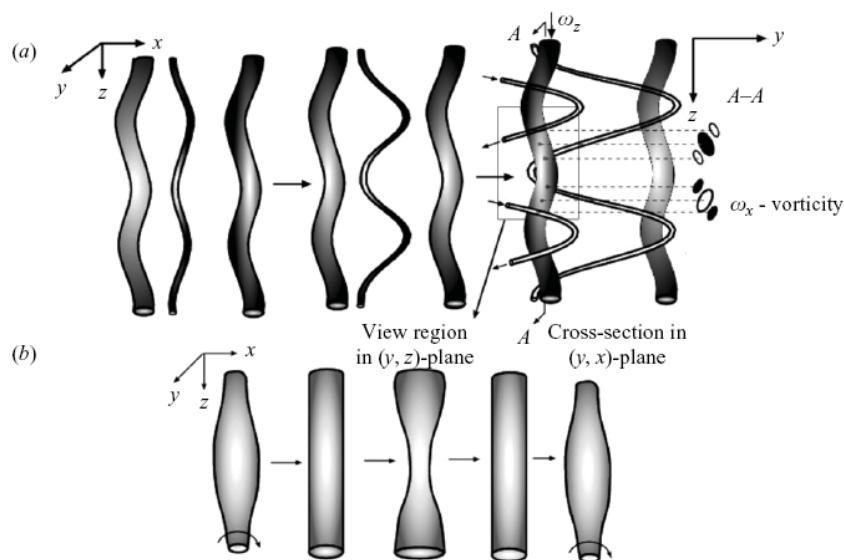


Fig. 1. Sketch of spatial development of different three-dimensional disturbances: (a) bending, (b) bulging.

In our recent experimental work [12,18,19] a mixing layer was perturbed in three-dimensions by using oscillating ‘chevron’-shape flapper, thus introducing spanwise disturbances along with the streamwise ones. The measurements revealed formation of either bending or bulging of KH rolls. An unexpected result was observed when flapper fluctuations magnitude was doubled from $A=1.5\text{mm}$ to $A=3\text{mm}$. This did not lead to a faster growth of the mixing layer thickness due to larger perturbation amplitude, as we expected. On the contrary, the amplitude growth was slowed down. At the same time, the mixing layer characteristics, such as cross-flow position of the average mean velocity value y_0 (y_0 is the cross-flow coordinate where the mean velocity is equal to a half of the sum of free stream velocities in the lower and upper borders of the mixing layer) and the momentum thickness θ , exhibited qualitatively different dependence on the spanwise coordinate. At lower flapper amplitude the y_0 position oscillated while the momentum thickness remained almost a constant. At larger amplitude we observed oscillations of θ in the spanwise direction and almost a constant value of y_0 . We assumed that larger flapper amplitude triggers the bulging instability instead of the bending one. Further observations revealed additionally that when the flapper was static the spanwise oscillations of y_0 were even stronger than in the case of 1.5mm amplitude of the flapper oscillations, while the momentum thickness did not change across the span. Due to its geometry, steady Chevron flapper generates strong static spanwise perturbations responsible for formation of translational instability, while its oscillations result in additional oblique initial perturbation generating bulging. Further increase of the oscillations amplitude from 1.5 mm to 3 mm leads to a prevailing role of bulging generated perturbations, which results in observed variations of y_0 simultaneously with approximate homogeneity of the momentum thickness in spanwise direction. Similar observations were reported by Bell & Mehta [8], but no explanation was provided.

In our computational modeling we studied development of 3D instabilities by introducing a 3D perturbation at the stages of under saturated and saturated KH billow, but before starting of a rollup or pairing. According to Pierrehumbert & Widnall [1], a perturbation responsible for bending should have a spanwise vorticity component antisymmetric in the cross-flow direction, and a symmetric one for bulging. Basing on this prediction we studied evolution of the symmetric and antisymmetric perturbations and had found that they really lead to bending or bulging of KH rollers. However, the result, i.e., bending or bulging, depends not only on the symmetry in cross-flow direction, but also on the phase shift of the initial perturbation in the streamwise direction when an oblique wave is generated, and on the choice of which Fourier mode is perturbed, i.e., purely spanwise or oblique. Thus, by switching between spanwise or oblique initially perturbed wave, or by placing the perturbation amplitude maximum inside the roller or inside the braid, we can switch between the bending and bulging instabilities. It should be emphasized that dependence of three-dimensional evolution of the mixing layer flow on initial disturbances is well documented (see, e.g., [8,9,19]). Here we show how a controlled initial disturbance can be used to switch between the bulging and bending modes.

Above observations were made for the fully 3D formulation where KH rollers were developing in time. Therefore it remained unclear whether growth of either bending or bulging results from a linear instability, in a complete analogy with the Stuart vortices, or time evolution of the billows and nonlinear interactions should be taken into account for explanation of the phenomena. To answer this question we repeat the above numerical modeling taking (i) small perturbation amplitudes to ensure linear initial growth, and (ii) KH billows frozen at two time moments corresponding to under saturated and saturated roller. This approach resembles one used [20]. The simulation with frozen billows shows growth of the bending and bulging modes in complete consistence with the fully non-linear modeling. This shows that bending and bulging can be interpreted as a result of linear instability of a combined flow consisting of mean flow and frozen KH billow. Moreover, this numerical exercise and monitoring the Fourier modes amplitudes allow us to conclude that development of both instabilities results from the triple interaction of the Fourier

modes (1,0), (0,1) and (1,1), where mode (1,0) represents the finite amplitude frozen KH billow and the two-dimensional base flow is a combination of the above mode (1,0) and the mean parallel flow that can be generalized as mode (0,0). The finite amplitude of the frozen KH billow is of order $O(1)$ as the mean flow, while two others modes (0,1) and (1,1) are of order $O(\varepsilon)$ at least at initial stages of the three-dimensional perturbations growth.

The following bulk of the paper is organized as follows. Formulation of the problem and a short description of numerical technique are given in Section 2. Numerical results obtained for the full and frozen-billow models are described in Section 3. All the results are discussed in Section 4, after which the concluding remarks are given.

2. Formulation of the problem and numerical method

We consider flow of Newtonian incompressible fluid described by the dimensionless momentum and continuity equations

$$\frac{\partial \mathbf{v}}{\partial t} + (\mathbf{v} \cdot \nabla) \mathbf{v} = -\nabla p + \frac{1}{Re} \Delta \mathbf{v}, \quad \nabla \cdot \mathbf{v} = 0 \quad (1,2)$$

in a three-dimensional rectangular box $0 \leq x \leq \lambda_x$, $-H \leq y \leq H$, $0 \leq z \leq \lambda_z$, where $\mathbf{v} = (u, v, w)$ is velocity and p is the pressure. The initial dimensional velocity distribution is defined as $\tilde{u} = U_{max} \tanh(y/\delta)$, where δ is the mixing layer thickness. Equations (1) and (2) are rendered dimensionless using δ , U_{max} , δ/U_{max} and ρU_{max}^2 as the scales of length, velocity, time and pressure, respectively. We assume periodicity in the x - and z - directions and vanishing of shear stresses at $y = \pm H$. Since the base initial flow is directed along the x -coordinate we refer to the velocity components u , v , and w and the corresponding directions as streamwise, normal and spanwise, respectively.

To visualize the evolution of mixing layer flow and similarly to [3] we add also a passive scalar T , whose evolution is described by a transport equation

$$\frac{\partial T}{\partial t} + (\mathbf{v} \cdot \nabla) T = \frac{1}{Pe} \Delta T, \quad (3)$$

where Pe is the Peclet number. The initial distribution of the passive scalar is given by the hyperbolic tangent $T = \tanh(y/\delta_T)$, where δ_T is the temperature layer thickness. In the following $\delta_T = \delta$. Similarly to the velocity field we prescribe periodicity conditions in the x - and z - directions and vanishing of $\partial T / \partial y$ at $y = \pm H$.

The numerical solution of the problem is carried out by mixed spectral/finite-difference method of [21]. Each scalar variable $f(x, y, z, t)$ is represented as truncated Fourier series

$$f = \sum_{|m| < M} \sum_{n=0}^{N-1} \left[f_{nm}^c(t, y) \cos\left(2\pi n \frac{z}{\lambda_z}\right) + f_{nm}^s(t, y) \sin\left(2\pi n \frac{z}{\lambda_z}\right) \right] \exp\left(2\pi i m \frac{x}{\lambda_x}\right) \quad (4)$$

Since the result of summation in eq. (4) must be real we impose an additional constraint on the coefficients f :

$$f_{n,m}^c = (f_{n,-m}^c)^*, \quad f_{n,m}^s = (f_{n,-m}^s)^*, \quad (5)$$

where asterisk denotes complex conjugation. Substitution of the series (4) in the equations (1)-(3) and calculation of the corresponding Galerkin projections in the x - and z - directions yield a system of non-linear PDEs for calculation of the y - and time-dependent coefficients f . We apply the finite difference method with the hyperbolic tangent mapping function to resolve in the y -direction. The time integration is carried out using a semi-implicit Runge-Kutta scheme [21].

In the following we refer to every term of the series (4) as a (m,n) mode $f_{m,n}$ of a function f . For example, the (m,n) mode of the streamwise velocity is defined as

$$u_{m,n}(x, y, z, t) = \left[u_{nm}^c(t, y) \cos\left(2\pi n \frac{z}{\lambda_z}\right) + u_{nm}^s(t, y) \sin\left(2\pi n \frac{z}{\lambda_z}\right) \right] \exp\left(2\pi i m \frac{x}{\lambda_x}\right) + c. c. \quad (6)$$

with *c.c.* standing for the complex conjugated terms. Clearly, the coefficients f_{nm}^c and f_{nm}^s , and in particular the coefficients u_{nm}^c and u_{nm}^s in eq. (9), are real, while each of the (m,n) modes is a complex function if $m \neq 0$. The modes corresponding to $m = 0$ describe perturbations that change in the spanwise plane and are uniform along the streamwise direction.

The amplitude F_{mn} of a (m,n) mode of a function f is defined as

$$F_{mn}^2 = \frac{1}{\lambda_x \lambda_z} \int_0^{\lambda_x} dx \int_0^{\lambda_z} dz \int_{-H}^H f_{mn}^2(x, y, z, t) dy \quad (7)$$

In addition we define the total amplitude of modes having a particular spanwise wavenumber F_n^S and the total amplitude of all modes F^{3D} as

$$(F_n^S)^2 = \sum_{m=-M}^M F_{mn}^2, \quad (F^{3D})^2 = \sum_{n=0}^N (F_n^S)^2 \quad (8)$$

Borders of the computational domain are chosen according to experiments of [22] and are set to $\lambda_x=15$, $\lambda_z=10$, and $H=20$. This yields the ratio between spanwise and streamwise wave lengths $\lambda_z/\lambda_x = 10/15 = 0.66$, which corresponds to the optimal value obtained in [1] for Stuart vortices. In most of numerical runs the solution was computed using 64 spectral modes in streamwise and spanwise directions and 128 grid points in y -direction. In some limited number of runs 128 spectral modes and 192 grid points are used. This increase of the resolution drastically changed the time of the run but did not affect significantly the final results.

To characterize developed mixing layer flow we use also its momentum thickness θ and position of the zero streamwise velocity y_0 . Taking into account that minimal and maximal dimensionless velocities are equal to ± 1 , the momentum thickness is defined as

$$\theta(x, z, t) = \int_{-H}^H \frac{u - U_{min}}{U_{max} - U_{min}} \left[1 - \frac{u - U_{min}}{U_{max} - U_{min}} \right] dy = \frac{1}{4} \int_{-H}^H (1 - u')(1 + u') dy \quad (9)$$

Where u' is the mean velocity profile shifted relatively to $(U_{min} + U_{max})/2$ and normalized by velocity difference $(U_{max} - U_{min})/2$ [22]. The experimental velocity profile in the vicinity of the splitter edge fits satisfactory the hyperbolic tangent function used in the computations as the initial velocity profile. The position y_0 is defined by the equation

$$u'[x, y_0(x, z, t), z, t]=0 \quad (10)$$

Following former and recent experiments [12,22] where perturbation was introduced at the edge of the splitter plate by a periodically oscillating flapper, we introduce small-amplitude perturbations of normal velocity v in the basic plane-parallel flow. In the computations described below we perturb $(1,0)$ mode of v to obtain an evolution of primary Kelvin-Helmholtz billows, and then perturb additionally the modes $(0,1)$ and $(1,1)$. Amplitudes of these modes were chosen to be symmetric or antisymmetric with respect to the midplane $y = 0$ and were defined by an even or odd function of y , respectively:

$$v_{sym}(y) = \begin{cases} A[1 - y^2]sech(y), & y \leq 1 \\ 0, & y > 1 \end{cases} \quad (11)$$

$$v_{asym}(y) = \begin{cases} A[1 - y^2]sech(y)tanh(y), & y \leq 1 \\ 0, & y > 1 \end{cases} \quad (12)$$

The amplitude A in eqs. (11) and (12) is defined as $A = A_0 e^{i\alpha}$, where A_0 is a small positive and real value, α defines a phase shift in the x -direction. The phase shift is used to place maximum of a streamwise wave either in the region of a billow or a braid.

All the numerical experiments described below were carried out in the following way. First, we started with a perturbed two-dimensional $(1,0)$ mode to obtain the KH rollup in the (x,y) plane of the mixing layer. Evolution of a 2D KH billow is illustrated in Figs. 2-4. Then all the two-dimensional modes $(m, 0)$ were frozen at a certain time, thus fixing a snapshot of the developing KH billow as a base state for the

further investigation. Also all the non-linear interactions of 2D modes $(m, 0)$ with other 3D modes were forcefully canceled. Then three-dimensional perturbations of modes $(0,1)$ or $(1,1)$ were introduced and the evolution of three-dimensional perturbations was studied. This evolution involves both the exponential growth of perturbation amplitudes and all possible non-linear interactions of all three-dimensional modes. This approach allows us to study the response of the mixing layer flow with developed primary rolls, both under- and over-saturated, to different three dimensional initial perturbations. Apparently, it must be started from a small-amplitude initial perturbation and remains meaningful as long as amplitudes of three-dimensional modes do not reach the order of amplitude of primary rolls.

3. Results

Non-linear evolution of the primary KH instability is illustrated in Figs. 2-4. Evolution of the amplitude of the primary 2D KH mode is shown in Fig. 2. Snapshots of isolines of the passive scalar T and spanwise vorticity component are shown in Figs. 3 and 4, respectively. Being the most unstable linear mode the primary KH billow grows exponentially during a certain time interval. When the roll up of the mixing layer increases (Figs. 3 and 4) the velocity inside the roll becomes of the same order of magnitude as the mean velocity of the base flow. At this stage the roll amplification terminates, and the amplitudes start to decrease. One observes that the KH rollup reaches saturation. At the same time the thickness of the mixing layer increases and its value becomes such that the base hyperbolic tangent base flow profile becomes linearly stable. Further development of the roll can be characterized by changes in its shape and a slow decrease of the velocity amplitudes (Fig.2). Actually, the roll energy decreases and there might be even energy transfer from the roll to the mean flow which is often observed in experiments and is also confirmed in this work (Fig. 2).

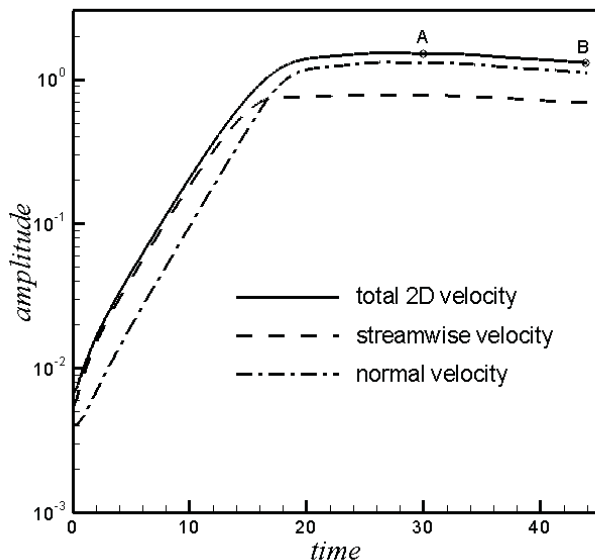


Fig. 2. Evolution of the amplitude of 2D perturbation of the primary base state for $Re = 250$.

The exponential growth of perturbations, characterized by the parameter β , can be separated into different time ranges corresponding to different instability stages. At the very beginning of the run (~ 2

time units) the growth is very steep followed by a rapid expansion of the layer thickness. The slope is characterized by $\beta \approx 30\%$. This value has been reported previously in [3]. When entering the later stage the growth rate drops by approximately a half ($\beta \approx 15\%$) and remains almost constant for a considerable time until the primary roll forms completely. In the calculations described below the 3D-perturbations are added at two different times: 30 and 44 time units. At $t = 30$ the primary rolls do not overlap, while at $t = 44$ the subsequent rolls overlap and oversaturation takes place (see Figs. 3 and 4). Comparing of the growth rate of 3D modes at different times we conclude that they do not depend the saturation stage of the primary roll.

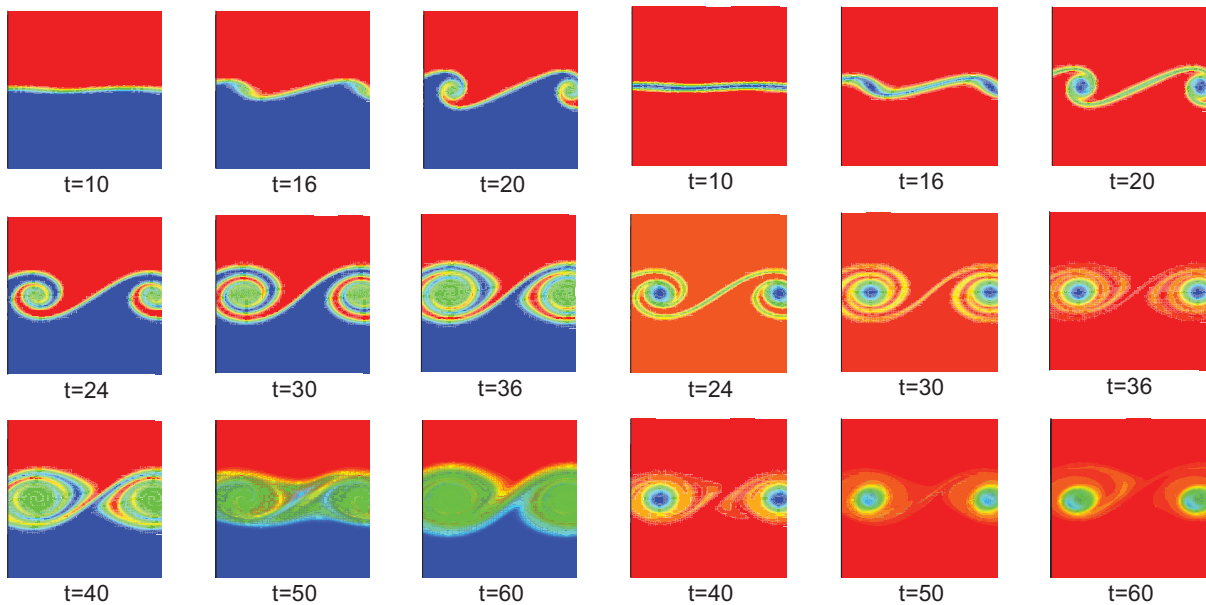


Fig. 3. Snapshots of isolines of the passive scalar T corresponding to a developing 2D flow at different times for $Re = 250$.

Fig. 4. Snapshots of isolines of z -vorticity of the developing 2D flow at different times for $Re = 250$.

Time moments, at which the primary roll was frozen, perturbed 3D modes, and the perturbation profiles (symmetric or asymmetric) for all the runs described below are summarized in Table 1. Figures 5 and 6 show time evolution of amplitudes of the components (0,1) and (1,1) for the 7 runs defined in the Table 1, in which either symmetrical (0,1) or antisymmetrical initial 3D perturbation (1,1) were introduced at different times. The initial perturbation amplitude was 10^{-3} in all runs.

First we describe runs corresponding to the developed, but not saturated primary KH roll at $t=30$. When the initial perturbation is defined by the mode (0,1) and its y -profile is *symmetric*, growth of the secondary disturbance is very fast (Fig. 5, run 1) and the primary roll is subject to bending. Another run with the same initial (0,1) mode but with an *antisymmetric* y -profile leads to a significantly slower growth (Fig. 5, run 2) and bulging of the primary roll is observed. Difference in the growth rates is indicated also by the values of β in Table 1. Also, the antisymmetric y -profile causes strong undulations of the amplitudes. Note also, that the excitation of the mode (0,1) causes a similar growth of the mode (1,1) (Fig.

6, runs 1 and 2), which is a result of the triad interaction of the modes (0,1) and (1,1) of the order $O(\varepsilon)$ with the frozen mode (1,0) of order $O(I)$.

Table 1. Summary of runs

Number of run	Time of switching on of 3D perturbation	type of perturbation	initially perturbed modes	Phase shift, α	β	Resulting structure
1	30	sym	0,1	0	5%	bending
2	30	asym	0,1	0	2%	bulging
3	30	asym	1,1	0	5%	bending
4	30	sym	1,1	0	2%	bulging
5	30	asym	1,1	90°	2%	bulging
6	44	sym	0,1	0	5%	bending
7	44	asym	0,1	0	2%	bulging

When the mode (1,1) is excited first, contrarily to the (0,1) mode excitation, we observe a rapid amplitude growth in the case of the *antisymmetric* y -profile (Table 1 and Fig. 6, run 3). Similarly to the above observations, this rapid growth leads to the bending of primary roll. When the initial perturbation profile is symmetric (Table1, run 4), we again observe a slower amplitude growth with undulations (Fig. 6, run 4) that leads to the bulging. As in the previous case we observe a similar growth of the mode (0,1) resulting from the triad interaction of the mode (1,1) and (0,1) of the order $O(\varepsilon)$ with the frozen mode (1,0) of order $O(I)$.

When the initial perturbation of the mode (1,1) is shifted by $\alpha = 90^\circ$ in the x -direction the behavior of the above initial perturbations switches in the case of *antisymmetric* y -profile. Namely, the shifted mode with $\alpha = 90^\circ$ grows slowly, exhibit undulations, and leads to the bulging (Table 1, run 5), unlikely the same excitation with $\alpha = 0^\circ$, that exhibits a fast growth and leads to the bending (Table 1, run 3).

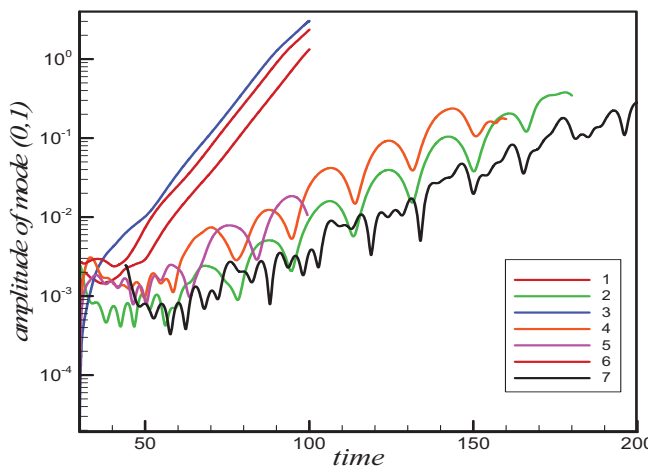


Fig. 5. Time evolution of the mode (0,1) for the 7 runs defined in Table 1.

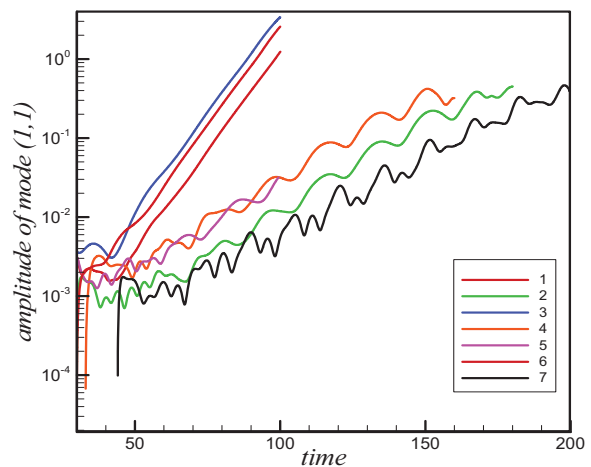


Fig. 6. Time evolution of the mode (1,1) for the 7 runs defined in Table 1.

Runs 6 and 7 in Table 1 correspond to the oversaturated primary KH roll frozen at $t=44$. Here we report only two runs with the symmetric and antisymmetric excitation of the mode (0,1), that also lead to either fast growth with bending or slow growth with bulging

The bending and bulging instabilities are illustrated by snapshots of isolines of the passive scalar T and the spanwise vorticity component Ω_z in Figs. 7-10. In these figures we show results obtained with the excitation of (0,1) mode only, since all other cases exhibit similar behavior. Note that the Prandtl number is equal to 1 and therefore the governing equations for Ω_z and T are similar. At the same time contours shown in Figs. 7-10 differ significantly, which is a result of different initial profiles and boundary conditions. The development of bending is clearly seen at the snapshots corresponding to shorter times in Figs. 7 and 8. Similarly, the bulging shape can be observed in Figs. 9 and 10. When the energy of 3D-modes becomes large, the contours become strongly distorted (Figs. 7-10). It can be observed also that the contours change drastically with the change of the relative location of a cross section in the streamwise direction. In spatially developing mixing layer, which is typical for experimental studies of free shear flows, it would mean a strong variation of these variables at different phases of the flapper fluctuations.

Isosurfaces of the streamwise vorticity ($\Omega_x = \partial w / \partial y - \partial v / \partial z$) are shown in Figs. 11 and 12 for the bending and bulging instabilities, respectively. The primary KH roll is illustrated in these figures by isolines of the scalar T plotted in the midplane $z = 0$. In the case of bending instability the streamwise vorticity starts to grow at the roll edges and is absent in the center of the roll. At earlier times the vorticity is antisymmetric with respect to the midplane $z = 0$, however at later times, e.g., at $t=94$ (Fig. 11), the antisymmetry breaks. Note that at the early stages ($t=32$) the streamwise vorticity does not develop at the mid-braid region and at the roll center. The large values of streamwise vorticity located near the roll edge and at the mid-braid emphasize a relative thickness of the braid during this stage of evolution. Evolution of the mixing layer leads to a fast growth of vorticity intensity and to evolving of strong vortices within the roll and in the braid region, as is it seen at $t=56$ (Fig. 11).

Fast increase of streamwise vorticity intensity can be observed at later times, $t=78$ and 94 (Fig. 11). The growth takes place both in the central plane of the roll and of the braid. For the time interval of 22 time units the intensity has been magnified almost in order of magnitude, and then gained another order of magnitude after 18 next time units. Note that the amplification of the streamwise vorticity takes place not only at the centers of primary roll but also at their periphery. We can speculate that a rib vortex, which is initiated in the braid plane reaches the primary roll edges. Since the primary roll is frozen the development of the secondary streamwise vorticity at short times is essentially a linear process. It includes the triad interactions of the primary roll, which can be represented as the mode (1,0) of order 1 and two secondary modes, (0,1) and (1,1) that are of order ε , which is equal to 10^{-3} in our calculations. The interactions of each of the secondary modes with the primary mode are the only ones essential. The other secondary mode is generated through this interaction when the first one is initially excited. The cross-interaction of the two secondary modes is not of any importance at the linear stage since it is of the order of ε^2 .

At larger times, when the intensity of secondary 3D vortices become approximately of the order of the primary 2D roll ($t=94$, Fig. 11) the isosurfaces of the secondary streamwise vorticity shrink in the spanwise direction and their size considerably decreases. Their cross-section reminds more and more cross-section of rib vortices. The secondary streamwise vorticity arriving from the braid region and that developing within the primary roll become tilted, which can be attributed already to the development of non-linear effects.

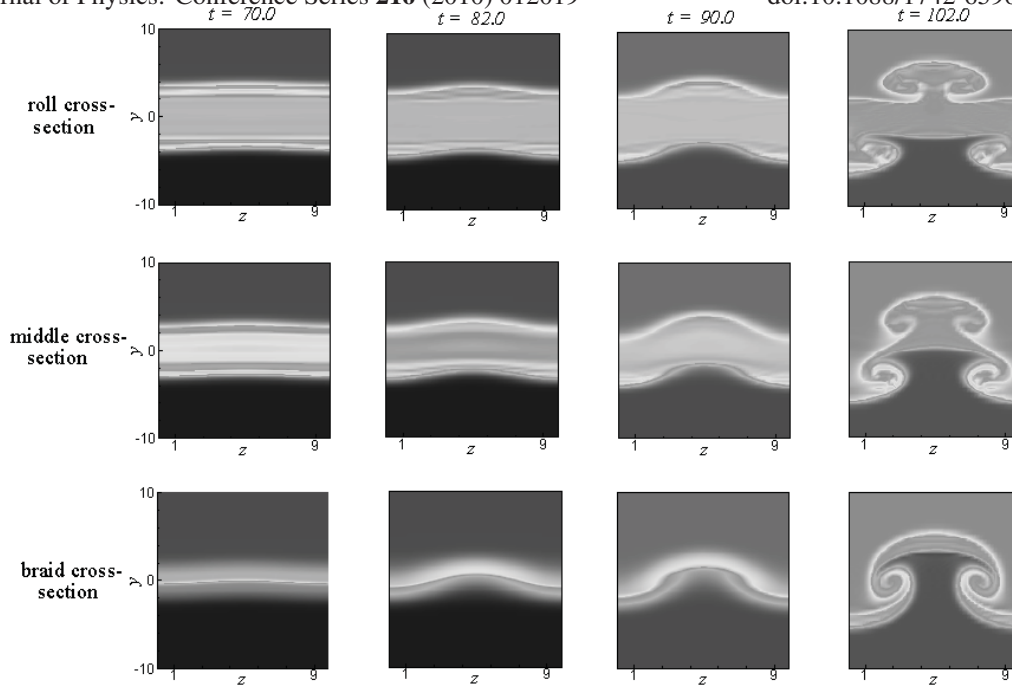


Fig. 7. Isolines of the passive scalar T in characteristic spanwise planes. Snapshots at $t = 70$ and 82 correspond to the initial bending instability. Snapshots at $t = 90$ and 102 correspond to the developing collapse of a 3D structure.

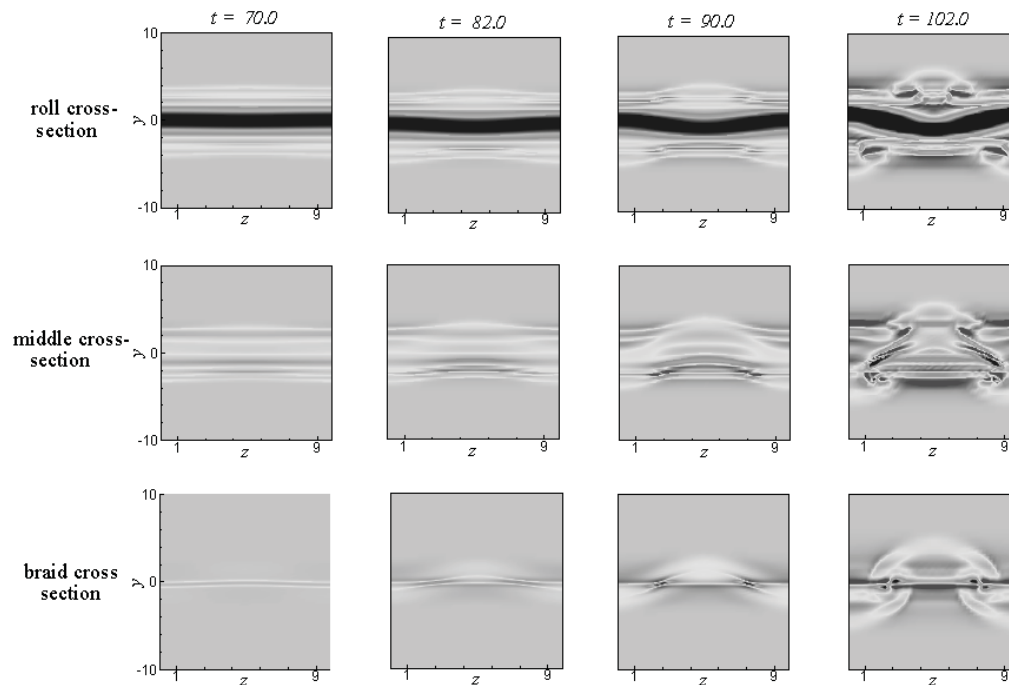


Fig. 8. Isolines of the spanwise vorticity component in characteristic spanwise planes. Snapshots at $t = 70$ and 82 correspond to the initial bending instability. Snapshots at $t = 90$ and 102 correspond to the developing collapse of a 3D structure.

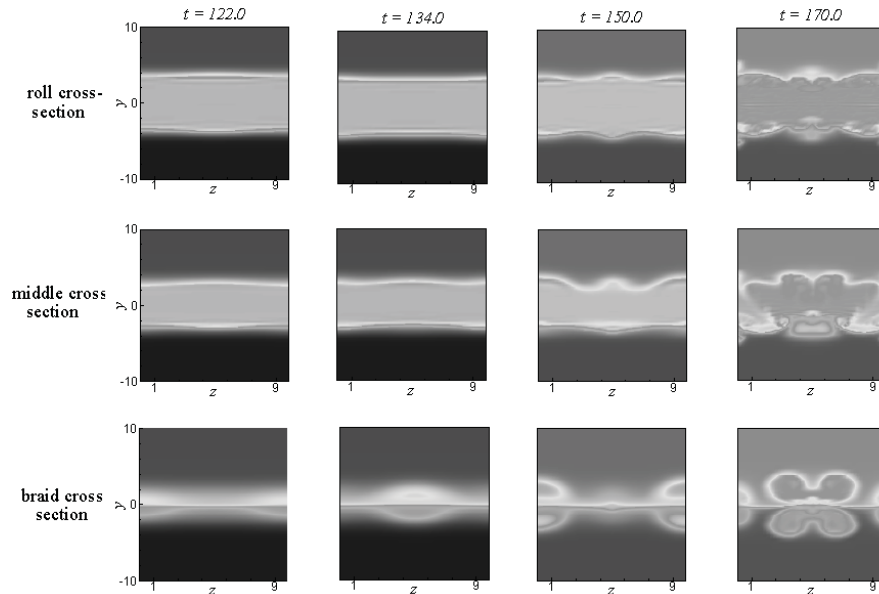


Fig.9. Isolines of the passive scalar T in characteristic spanwise planes. Snapshots at $t = 122$ and 134 correspond to the initial bulging instability. Snapshots at $t = 150$ and 170 correspond to the developing collapse of a 3D structure.

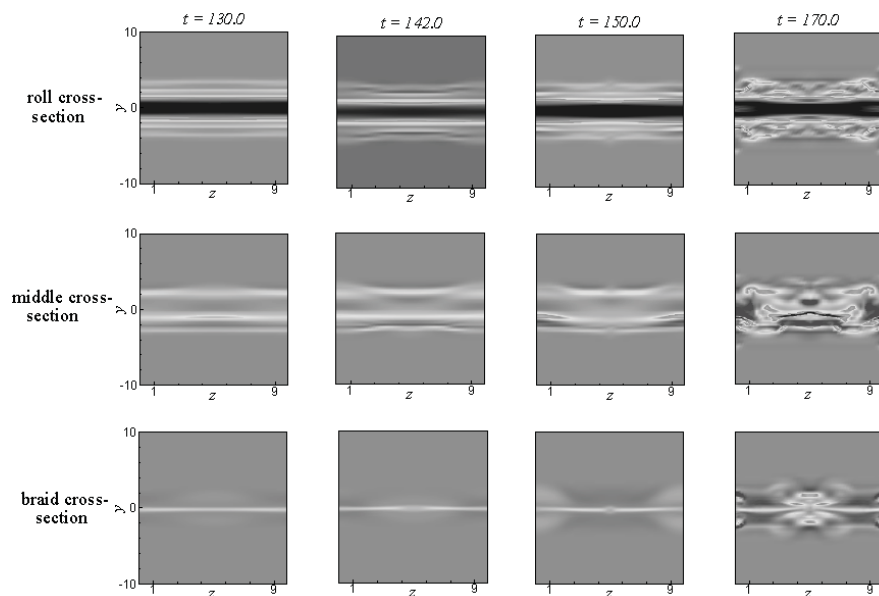


Fig.10. Isolines of the spanwise vorticity component in characteristic spanwise planes. Snapshots at $t = 130$ and 142 correspond to the initial bulging instability. Snapshots at $t = 150$ and 170 correspond to the developing collapse of a 3D structure.

The evolution of the streamwise vorticity differs significantly from that shown in Fig. 11 if the secondary instability is excited by a slow bulging mechanism. At relatively short times, e.g., $t=72$ in Fig. 12, a large number of vorticity minima and maxima in the primary roll are related to the streamwise vorticity growth within well-distinguished layers developing in the process of rolling up. As in the previous case the streamwise vorticity is antisymmetric with respect to the midplane $z = 0$. These antisymmetric pairs are observed for all cross-sections including the center of the braid section. The latter is of special importance since it indicates that no stretching of the vorticity lines develops in the linear regime. Thus, development of rib vortices typical for translation bending mode of secondary instability does not take place.

As in the previous case the streamwise vorticity grows with time (Fig. 12). At the same time the shape of the isolines does not change significantly during a rather long time period (compare $t=100$ and 140), and then is destroyed at later times by non-linear mechanisms ($t=172$). Obviously, when the bulging mode develops the streamwise vorticity grows significantly slower than in previously considered case when the translational bending mode and rib vortices are being developed.

Stretching and folding of vorticity lines are shown in Figs. 13 and 14. The first frame of Fig. 13 illustrates the initial locations of the lines determined by the largest vorticity intensity. These lines are located at the primary roll center and at the center of the braid. Further stretching of vorticity lines in the case of bending (Fig. 13) leads to a development of primary roll bending and rib vortices. Hair pin structures appear at larger times. The red color indicates their penetration into the upper semi-volume, $y > 0$, and blue into the lower.

A typical development of bulging is illustrated in Fig. 14. When the vorticity lines at the roll center attain a bulged shape their counterparts in braid region remain practically unchanged. At later times the non-linear effects become important and collapse of the primary roll occurs, generating rings. The vorticity lines in the braid region are stretched and bended in a very complicated manner with a symmetry breaking already observed for the streamwise vorticity. Note that in the case of bending the latter structure appears mostly in the lower semi-volume.

Figure 15 presents spanwise distribution of the momentum thickness θ and the lateral coordinate y_0 corresponding to the zero value of mean streamwise velocity at different times of mixing layer evolution in the case of bending instability. These values have been computed after the averaging over the streamwise coordinate has been made. As follows from Fig. 15 no variation of θ and y_0 is observed till $t \approx 50$. At larger times both values θ and y_0 start to vary. At $t=58$ one does not observe strong spanwise variations of θ while y_0 attains a spanwise oscillation with the same spanwise spatial period as the initial perturbation. At larger times ($t=82$), the amplitude of y_0 oscillations increases significantly. The momentum thickness θ starts to vary as well, seemingly, at double frequency. At even higher values of time, $t=94$, the non-linear effects become strong and both variables vary in spanwise direction but not at the fundamental frequency. Very similar results were observed in the experiments [12] in the presence of oscillating Chevron flapper with amplitude of 1.5mm. At larger distances, the developing turbulent fluctuations in the experiments, which are not accounted for in the numerical simulations, change the spanwise distributions of both variables.

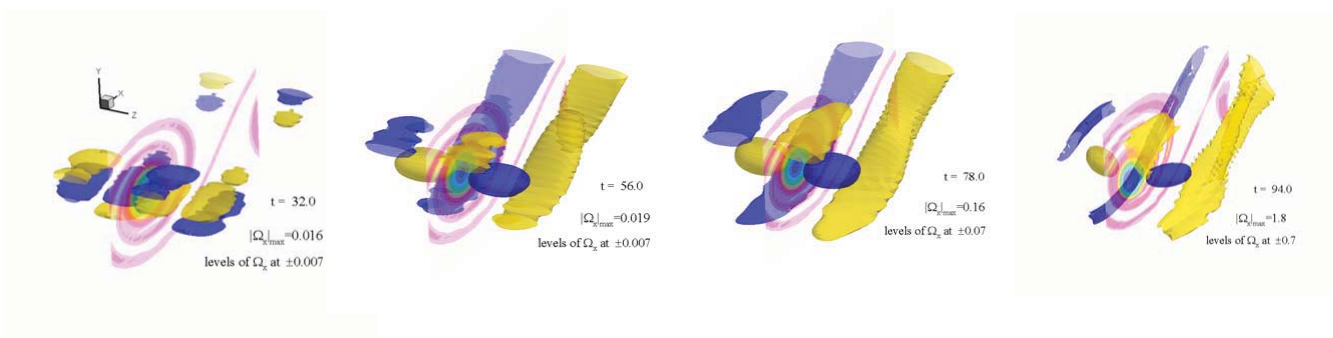


Fig. 11. Isosurfaces of the streamwise vorticity for bending instability. Parameters of run 1 (Table 1).

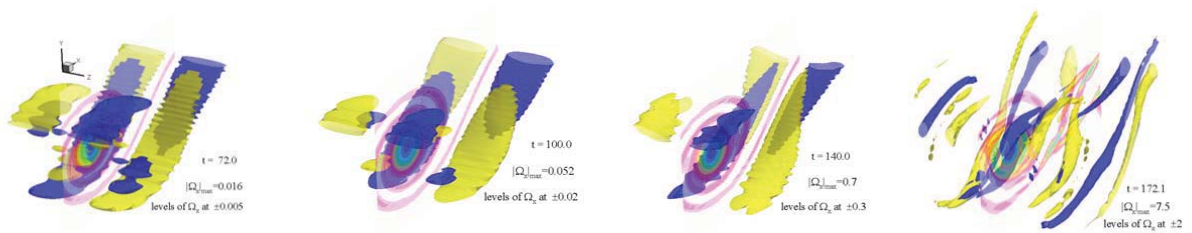


Fig. 12. Isosurfaces of the streamwise vorticity for bulging instability. Parameters of run 2 (Table 1).

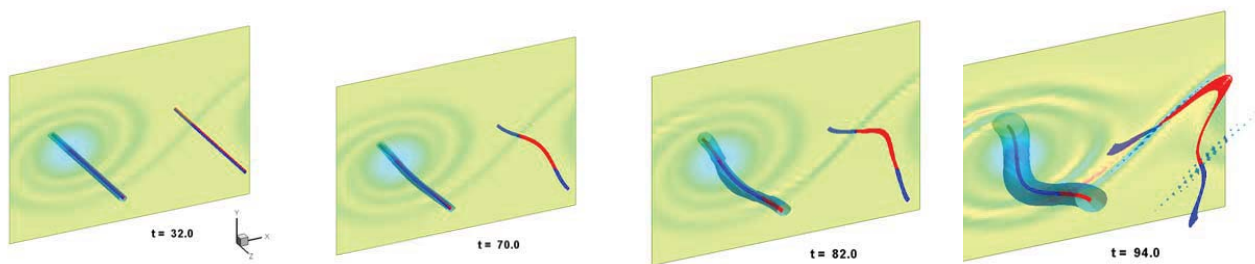


Fig. 13. Isosurfaces of the spanwise vorticity for bending instability. Parameters of run 1 (Table 1).

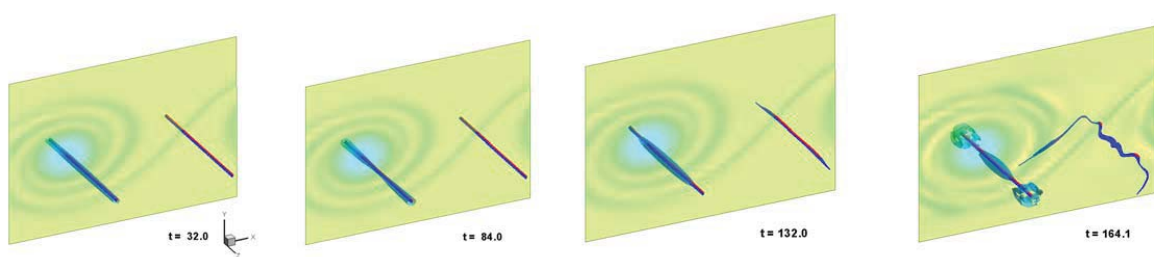


Fig. 14. Isosurfaces of the spanwise vorticity for bulging instability. Parameters of run 2 (Table 1).

Distributions of the momentum thickness θ obtained for bulging mode at several different times are shown in Fig. 16. As can be expected for the bulging mode, the position y_0 remains unchanged at all times and is not shown. We observe that, compared with the bending mode (Fig. 15), the momentum thickness noticeably oscillates in the spanwise direction at large times ($t=170$). In general, the bulging processes develop slower than the bending ones. In the experiments with chevron flapper it is impossible to obtain a separated bulging mode. Nevertheless, the increase of chevron flapper perturbation amplitude up to 3mm increased the relative contribution of bulging mode, which lead to a relative increase of the momentum thickness compared to the variation of y_0 [12].

The mean velocity and temperature profiles at the mid spanwise position $z=5$ are shown in Figs 17 and 18 for bending and bulging instabilities, respectively. The averaging was conducted over the entire streamwise spatial period. The vertical y -coordinate in these figures is normalized by velocity momentum thickness θ computed for the corresponding time. Since in these computations $Ri = 0$, there is no stratification and the temperature behaves as a passive scalar. The temperature is affected by velocity field but not vice versa. The velocity profiles remain smooth and the initial hyperbolic tangent profile keeps more or less its shape during the evolution. The profile of passive scalar varies significantly even during development of two-dimensional perturbations, $t=30$ (Figs. 17 and 18). At this time strong temperature gradients are observed at the mixing layer edges. Also in the mixing zone the temperature noticeably, so that local overturning of the profile can be noticed. Within the primary vorticity core these effects are expected to be stronger. Figure 3 indicates appearance of low temperature layers above layers with higher temperature. As expected with initial perturbations generating the bending mode, the mean profiles change faster (cf. Figs. 17 and 18). The lack of symmetry observed at greater times is most probably related to fast development of three-dimensional non-linear effects with time evolution.

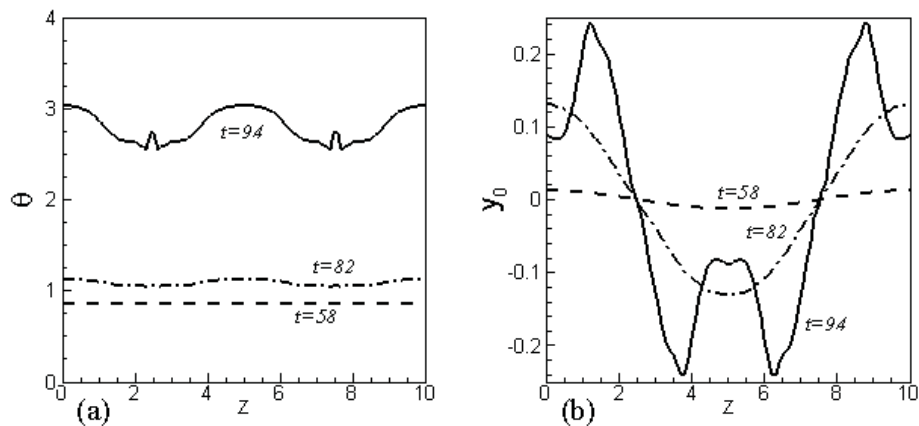


Fig. 15. Spanwise distributions of momentum thickness θ and the lateral coordinate y_0 corresponding to the zero value of mean streamwise velocity for bending instability (run 1 of Table 1).

The RMS distributions of amplitudes of all the three velocity components, temperature and spanwise vorticity are presented in Figs. 19 and 20 for the bending and bulging instabilities, respectively. The most interesting result in both cases is the observation of relatively strong streamwise and cross-stream velocity amplitudes penetrating into the potential velocity region while the temperature and streamwise vorticity are limited to the mixing layer region. The variation of temperature fluctuations is almost abrupt: it changes from relatively high values to almost zero at very short lateral distances. The spanwise velocity component emerges at greater time indicating evolution of three dimensional effects. At this specific spanwise coordinate, $z=5$, its lateral distribution is more symmetric for the bulging mode case

(Fig. 20). This is perhaps the reason for more symmetrical shape of temperature and spanwise fluctuations distributions.

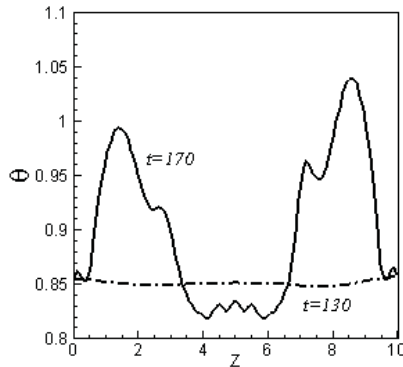


Fig. 16. Spanwise distributions of momentum thickness θ for bulging instability (run 2 of Table 1).

Velocity and temperature (averaged across XY plans) correlations along spanwise direction are presented in Figs. 21 and 22. The shape of these correlations is indicative for understanding of the secondary structures. In particular, when these correlations are close to unity the flow structure is two-dimensional, e.g., as obtained at a short time $t=30$. At longer times, this value deviates from unity, thus, demonstrating development of secondary 3D-structures. While the underlying processes are linear, the correlations exhibit sine-like variations ($t=58$ in Fig 21 and $t=102$ and $t=130$ in Fig. 22). Strong evolution of non-linear processes results in non-harmonic shapes of the correlations as can be noticed in Fig. 21 at times, $t=82$ and $t=94$ and in Fig. 22 at $t=170$. Two velocity components, streamwise and cross-stream, are *symmetric* in spanwise direction while the spanwise component is *antisymmetric*.

At longer times the spanwise periodicity remains unchanged for the bending mode but varies significantly in the bulging mode case ($t=170$, Fig. 22). This result may be important when correlations of coherent velocity components obtained in the experiments are considered. In particular, it can be used to determine the mode obtained in these experiments. The spanwise variation of correlation of streamwise velocity component is significantly larger than that of lateral velocity component. A similar result was observed also in experiments [12].

4. Discussion and conclusions

The computational approach adopted in the current study with two-dimensional and three-dimensional perturbations introduced into the mixing layer at different times allowed us to distinguish between evolution of primary two-dimensional roll and development of secondary three-dimensional structures. Although this distinction is somewhat artificial it helps to understand better the mechanisms of development of secondary 3D structures. In particular, this approach is justified by a faster amplification of 2D-primary roll and lower level of initial 3D perturbations. Due to these effects, the primary roll becomes dominant even in case when all perturbations *are excited simultaneously*. Also, it helped to understand how the symmetry features of initial perturbation affect evolution of secondary 3D structures. It must be emphasized that the actual perturbations considered here are composite due to triad interaction of the two initial secondary modes: (0,1) and (1,1) and the primary, independent on the spanwise coordinate, two-dimensional mode (1,0). The latter develops into the primary roll during the initial stage of evolution.

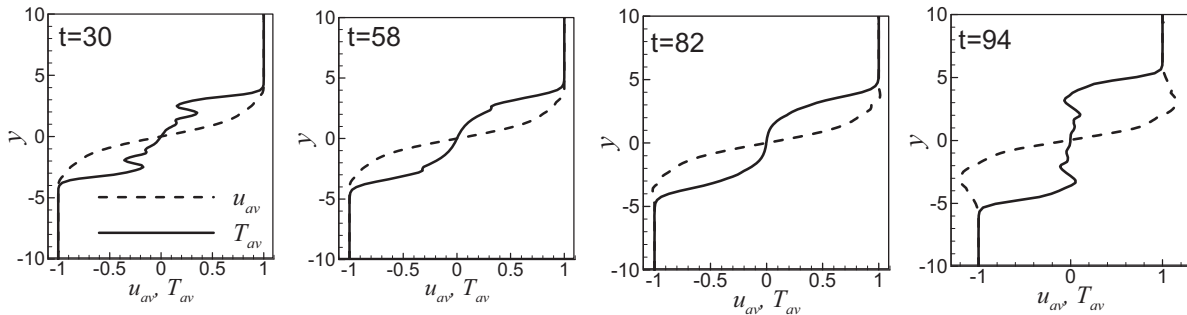


Fig. 17. Normalized mean velocity and temperature profiles at the mid spanwise position $z=5$ for bending instability (run 1 of Table 1).

As can be observed from Figs. 5 and 6 symmetry properties of secondary perturbations determine uniquely the mode of 3D instability: bending or bulging. The oversaturation of primary roll affects the rate of growth and in case of bulging mode the frequency of periodic oscillations during the growth, but secondary disturbances patterns remain qualitatively unchanged. When the bending mode develops, the rib and core vortices evolve while bulging mode results in a complicated structure of core vortices. No rib vortices are observed in the case of bulging.

When time is long enough the size of primary roll increases (oversaturation) and the successive primary rolls overlap. In this case velocity and shear in the middle of the braid are affected by the primary rolls (Figs. 3 and 4). The mushroom structure is observed at large times, e.g., starting from $t \approx 94$ for the case of Fig. 7. Similar mushroom structures were observed in some experimental studies (see, e.g., [7]). Also in measurements with SPIV system these structures were obtained when the smoke was not homogeneously spread across the plane. The continuous bulging structure breaks to separate rings at larger times (Fig. 8, $t=150$), similar to what was observed in [3].

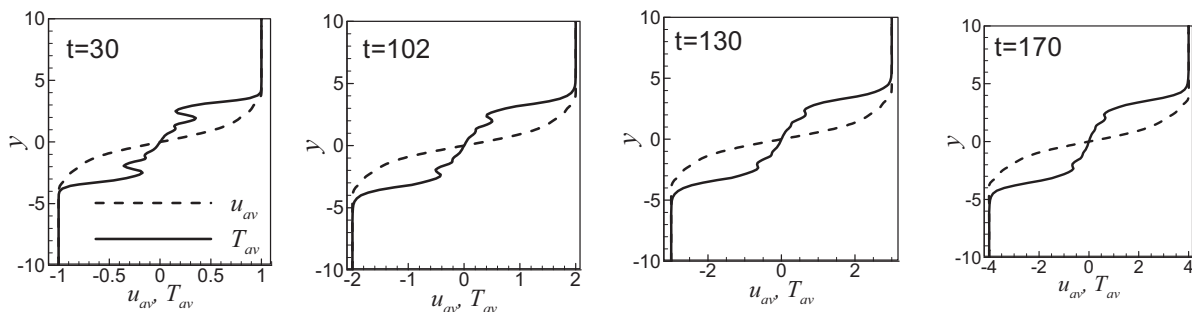


Fig. 18. Normalized mean velocity and temperature profiles at the mid spanwise position $z=5$ for bulging instability (run 2 of Table 1).

Evolution of streamwise vortices clearly shows generation of hair-pin vortices. It follows from Fig. 13 that stretching of braid lines, which are deprived of vorticity due to roll up process, is relatively fast and represents mechanism leading to formation of hair-pin vortices. These structures eventually interact with the primary rolls and results in their collapse and developing of strong turbulence within these cores. One can speculate that in the bending regime the 3D-turbulence develops in the peripheral region. In the bulging regime, where rib vortices do not develop and the instability occurs mainly in the core, the turbulence should develop within the core.

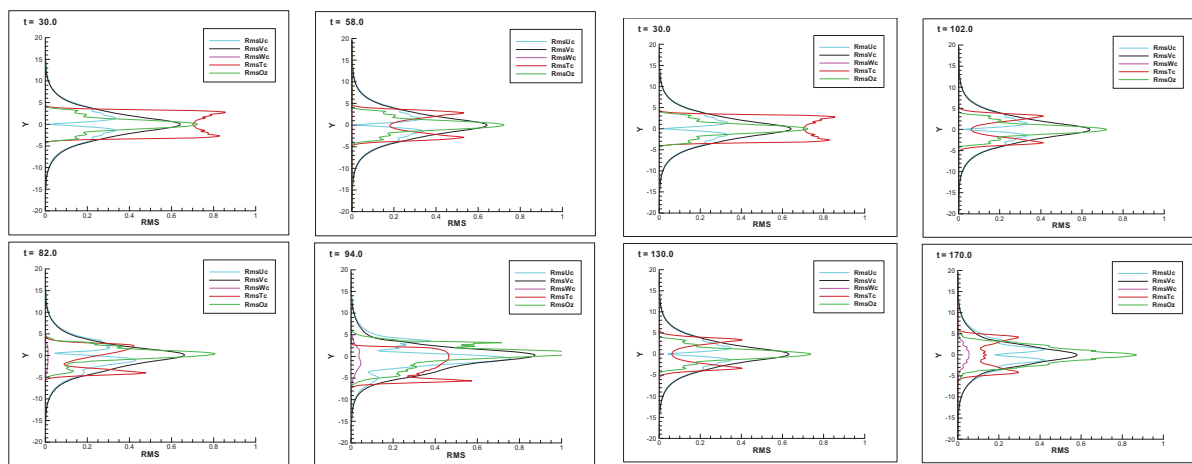


Fig. 19. RMS amplitudes of velocity components, temperature and spanwise vorticity for the bending instability, $z=5$.

Fig. 20. RMS amplitudes of velocity components temperature and spanwise vorticity for the bulging instability, $z=5$.

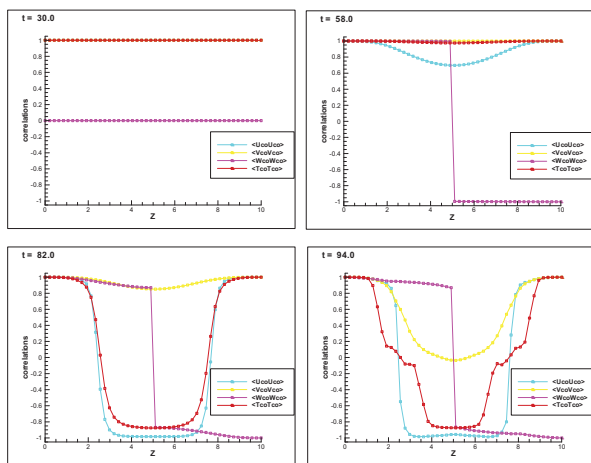


Fig. 21. Average velocity and temperature correlations in the spanwise direction. Bending instability.

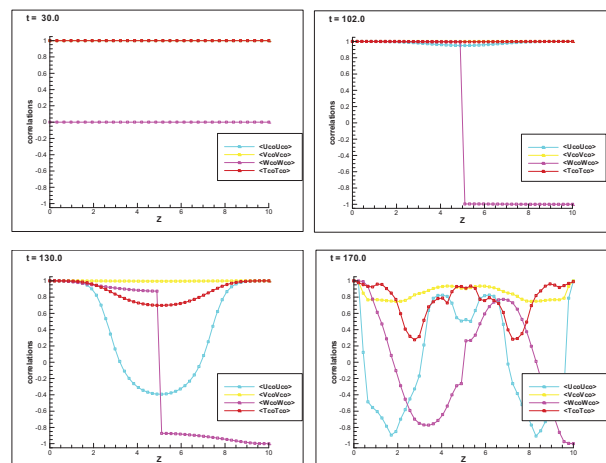


Fig. 22. Average velocity and temperature correlations in the spanwise direction. Bulging instability

Computational modeling of the fully nonlinear model with both two- and three-dimensional perturbations introduced in the flow reveals qualitatively similar instabilities development. At smaller times, the flow is mainly two-dimensional and the spanwise variations are relatively small. Depending on the kind of the three-dimensional perturbation, at longer time ($t=82$ and $t=130$ for bending and bulging, respectively) the flow becomes essentially three-dimensional. At even larger times ($t=94$ and $t=170$) when non-linear three-dimensional effects prevail the growth of perturbations becomes steeper (especially for the bending/translation mode) and the mixing layer diverges faster. It should be stressed that these computations did not account for the pairing, which can be of great importance at more advanced stages of mixing layer evolution. The whole non-linear three-dimensional evolution of the mixing layer flow takes place in a very good agreement with the experimental results [12]. More details on these calculations can be found in [23].

The main conclusion of the present study is that three-dimensional perturbations, harmonic in the streamwise and spanwise directions, enhance the primary (KH) instability and modulate the ensuing eddies along the span. The three-dimensional disturbances can be divided into two sets that differ by their cross-flow symmetry and streamwise phase, and lead to development of either bending or bulging instability. Perturbations belonging to the first set enhance the translative instability that bends the (initially spanwise-uniform) KH vortices and develop streamwise rib vortices. The second set of initial perturbations generates the bulging mode that leads to spanwise alteration of the KH billows width. Both sets create coherent streamwise vorticity within the rollers and braid regions, which lead to the development of streamwise vortex tubes (rib vortices and bent or bulging spanwise vortices) farther downstream. Both types of three-dimensional distortions of the primary spanwise rolls, bending and bulging, can be distinguished by spanwise variations of the momentum thickness θ and vertical position of the mean velocity y_0 . In the case of bending one observes almost constant θ and spanwise oscillations of y_0 . Conversely, the bulging leads to spanwise oscillations of θ and almost unaltered y_0 position.

The streamwise vortices become less coherent with time increasing. At longer times, when the non-linear effects become essential, they seem to disappear in the straining field existing between adjacent KH rolls (braid region), as well as becoming less regular and weaker within the rolls themselves. This might be an outcome of a strong interaction between spanwise KH type of rolls and streamwise vortex tubes. Before collapse of the rib vortices, very clear structures reminding hair-pin or lambda vortices are observed. This result might explain observation of such structures in real physical experiments.

The velocity profiles and all the parameters, such as momentum thickness and location of the mixing layer center (where streamwise velocity becomes zero) obtained using these profiles in the current experiments are in very good qualitative agreement with experimentally observed coherent structures in spite of the fact that computations are conducted for the temporally evolving mixing layer while the measurement were carried out for spatially developing one.

An interesting observation from this work is the strong linkage between the lateral perturbation nature (by means of symmetry) and the spanwise & streamwise modes (2D or 3D) to the instability type. This behavior has not been explained within the current study and might be worth further investigation.

Acknowledgements This work is supported by the Bi-National Science Foundation (Grant 2004087) and in part by the Israel Science Foundation (Grant 964/05).

References

- [1] Pierrehumbert R T and Widnall S E. 1982 The two- and three-dimensional instabilities of a spatially periodic shear layer *J. Fluid, Mech.*, **114** 59
- [2] Schoppa W, Hussain F and Metcalfe R W 1995 A new mechanism of small-scale transition in a plane mixing layer: core dynamics of spanwise vortices *J. Fluid Mech.* **298** 23
- [3] Rogers, M M and Moser R D 1992 The three-dimensional evolution of a plane mixing layer: the Kelvin-Helmholtz rollup *J. Fluid Mech.* **243** 183
- [4] Schoppa W, Hussain H S, and Hussain F 1993 Nonlinear instabilities of free shear layers: subharmonic resonance and three-dimensional vortex dynamics In *Nonlinear Instability of Nonparallel Flows* (ed. S.P. Lin et al.), pp. 251-280, Springer.
- [5] Jimenez J 1983 A spanwise structure in the plane shear layer *J. Fluid Mech.* **132** 319
- [6] Bernal L P and Roshko A. 1986 Streamwise vortex structure in plane mixing layers *J. Fluid. Mech.* **170** 499
- [7] Lasheras J C and Chol H 1988 Three-dimensional instability of a plane free shear layer: an experimental study of the formation and evolution of streamwise vortices *J. Fluid Mech.* **189** 53
- [8] Bell J H and Mehta R D, 1993 Effects of imposed spanwise perturbations on plane mixing layer structure *J. Fluid Mech.* **257** 33-63.
- [9] Nygaard K J and Glezer A 1994 The effect of phase variations and ceoss-shear on vortical structures in a plane mixing layer *J. Fluid Mech.* **276** 21
- [10] Tung S and Kleis S J 1996 Initial streamwise vorticity formation in a two-stream mixing layer *J. Fluid Mech.* **319** 251
- [11] Estevadeordal J and Kleis S J 2002. Influence of vortex-pairing location on the three-dimensional evolution of plane mixing layer *J. Fluid Mech.* **462** 143
- [12] Kit E, Wygnansky I, Friedman D, Krivonosova O and Zhilenko D 2007. On the periodically excited plane turbulent mixing layer, emenating from a jagged partition *J. Fluid Mech.* **589** 479
- [13] Metcalfe R W, Orszag S A, Brachet M E, Menon S and Riley J J 1987 Secondary instability of a temporally growing mixing layer *J. Fluid Mech.* **184** 207
- [14] Ashurst W T, and Meiburg E 1988 Three-dimensional shear layers via vortex dynamics *J. Fluid. Mech.* **189** 87
- [15] Caulfield C P and Peltier W R 1994 Three dimensionalization of the stratified mixing layer *Phys. Fluids* **6** 3803
- [16] Khac M D, Basdevant C, Hiêp-Lê T, and Dang-Tran K 1998. Topological and dynamical analysis of a three-dimensional mixing layer *Aerospace Sci. Technol.* **1** 13
- [17] Kit E, Krivonosova O, Zhilenko D and Friedman D 2005 Reconstruction of large coherent structures from SPIV measurements in a forced turbulent mixing layer *Experiments in Fluids* **39** 761
- [18] Kit E and Wygnanski I 2008 On periodically excited turbulent mixing layer created downstream of a plane chevron partition *Physica Scripta T*, doi:10.1088/0031-8949/2008/T132/014008.
- [19] Scott Collis S, Lele S K., Moser R D. and Rogers M M 1994 The evolution of a plane mixing layer with non-uniform forcing *Phys. Fluids* **6** 381
- [20] Klaassen G P and Peltier W R 1985 The onset of turbulence in finite-amplitude Kelvin-Helmholz billows *J. Fluid Mech.* **155** 1
- [21] Nikitin N V 1994 A spectral finite-difference method of calculating turbulent flows of an incompressible fluid in pipes and channels *Comp. Maths. Math. Phys.* **34** 785
- [22] Gaster M, Kit E and Wygnanski I 1985 Large-scale structures in a forced turbulent mixing layer *J. Fluid Mech.* **150** 23
- [23] Gerstenfeld D 2007 3D simulation of secondary instability modes of kelvin-helmholtz billows in plane mixing layer, M. Sc. Thesis, Faculty of Engineering, Tel-Aviv University, 77pp.